

# Interplay among helical order, surface effects and range of interacting layers in ultrathin films.

F. Cinti<sup>(1,2,3)</sup>, A. Rettori<sup>(2,3)</sup>, and A. Cuccoli<sup>(2)</sup>

<sup>(1)</sup> *Department of Physics, University of Alberta, Edmonton, Alberta, Canada T6G 2J1*

<sup>(2)</sup> *CNISM and Department of Physics, University of Florence, 50019 Sesto Fiorentino (FI), Italy. and*

<sup>(3)</sup> *CNR-INFM S<sup>3</sup> National Research Center, I-41100 Modena, Italy*

(Dated: February 13, 2022)

The properties of helical thin films have been thoroughly investigated by classical Monte Carlo simulations. The employed model assumes classical planar spins in a body-centered tetragonal lattice, where the helical arrangement along the film growth direction has been modeled by nearest neighbor and next-nearest neighbor competing interactions, the minimal requirement to get helical order. We obtain that, while the in-plane transition temperatures remain essentially unchanged with respect to the bulk ones, the helical/fan arrangement is stabilized at more and more low temperature when the film thickness,  $n$ , decreases; in the ordered phase, increasing the temperature, a softening of the helix pitch wave-vector is also observed. Moreover, we show also that the simulation data around both transition temperatures lead us to exclude the presence of a first order transition for all analyzed sizes. Finally, by comparing the results of the present work with those obtained for other models previously adopted in literature, we can get a deeper insight about the entwined role played by the number (range) of interlayer interactions and surface effects in non-collinear thin films.

PACS numbers: 64.60.an, 64.60.De, 75.10.Hk, 75.40.Cx, 75.70.Ak.

## I. INTRODUCTION

The study of low dimensional frustrated magnetic systems<sup>1</sup> still raises great interest, both in consequence of theoretical aspects, related to their peculiar critical properties<sup>2</sup>, and in view of possible technological applications<sup>3</sup>. Indeed, beside conventional ferromagnetic or antiferromagnetic phase transitions, in many new materials other nontrivial and unconventional forms of ordering have been observed<sup>4,5</sup>. A quantity of particular interest in this context is the spin chirality, an order parameter which turned out to be extremely relevant in, e.g., magnetoelectric materials<sup>6</sup>, itinerant MnSi<sup>7</sup>, binary compounds as FeGe<sup>8</sup>, glass transition of spins<sup>9</sup>, and XY helimagnets, as Holmium, Terbium or Dysprosium<sup>10</sup>. In the latter case, a new universality class was predicted because a  $\mathbb{Z}_2 \times SO(2)$  symmetry is spontaneously broken in the ordered phase<sup>2</sup>: In fact, when dealing with such systems, in addition to the  $SO(2)$  symmetry of the spin degrees of freedom  $\vec{S}_i$ , one has to consider also the  $\mathbb{Z}_2$  symmetry of the spin chirality  $\kappa_{ij} \propto [\vec{S}_i \times \vec{S}_j]^z$ .

For these rare-earth elements, the development of new and sophisticated experimental methods<sup>11</sup> has allowed to obtain ultra-thin films where the non-collinear modulation is comparable with the film thickness. Under such conditions the lack of translational invariance due to the presence of surfaces results decisive in order to observe a drastic change of the magnetic structures<sup>12</sup>. Recent experimental data on ultra-thin Holmium films<sup>13</sup> have been lately interpreted and discussed<sup>14,15</sup> on the basis of detailed classical Monte Carlo (MC) simulations of a spin Hamiltonian, which is believed to give a realistic modeling of bulk Holmium. Such Hamiltonian, proposed by Bohr et al.<sup>16</sup>, allows for competitive middle-range in-

teractions by including six different exchange constants along the  $c$  crystallographic axis, and gives a helix pitch wave-vector  $Q_z$  such that  $Q_z c' \simeq 30^\circ$ , where  $c' = c/2$  is the distance between nearest neighboring spin layers parallel to the  $ab$  crystallographic planes, henceforth denoted also as  $x - y$  planes, while  $z$  will be taken parallel to  $c$ . For  $n > 16$ ,  $n$  being the number of spin layers in the film, a correct bulk limit is reached, while for lower  $n$  the film properties are clearly affected by the strong competition among the helical pitch and the surface effects, which involve the majority of the spin layers. In the thickness range  $n = 9 - 16$ , i.e. right for thickness values comparable with the helical pitch, three different magnetic phases emerged, with the high-temperature, disordered, paramagnetic phase and the low-temperature, long-range ordered one separated by an intriguing, intermediate-temperature block phase, where outer ordered layers coexist with some inner disordered ones, the phase transition of the latter eventually displaying the signatures of a Kosterlitz-Thouless one. Finally, for  $n \leq 7$  the film collapses once and for all to a quasi-collinear order.

The complex phase diagram unveiled by such MC simulations awaken however a further intriguing question: to what extent the observed behavior may be considered a simple consequence of the competition between helical order and surface effects? I.e., is it just a matter of having such a competition or does the range of interactions also play a relevant role? Indeed, when the range of the interactions is large enough we have a greater number of planes which can be thought of as "surface planes", i.e. for which the number of interacting neighbors are significantly reduced with respect to the bulk layers; therefore, we expect that the larger the interaction range, the stronger should be the surface effects. But, at the same time, the same modulation of the magnetic order can

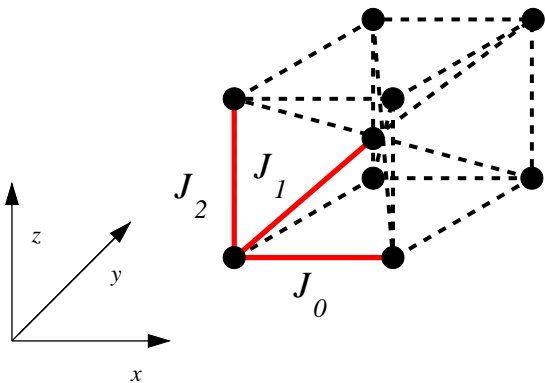


FIG. 1: (colors online) (a): body-centered tetragonal (BCT) lattice with  $J_0$  in-plane coupling constant, and out-of-plane  $J_1$ , and  $J_2$  competing interactions.

be achieved with different number of interacting layers: notably, nearest and next-nearest layers competitive interactions are enough to get a helical structure with a whatever pitch wavevector. Such observation gives us a possible way to solve the conundrum previously emerged, as we have the possibility of varying the range of interactions without modifying the helical pitch, thus decoupling the two relevant length scales along the film growth direction, and making accessible a range of  $n$  of the order of, or smaller than, the helical pitch, but still large enough that a substantial number of layers can behave as “bulk” layers. Therefore, while in the previous papers we have studied the properties of ultrathin magnetic films of Ho assuming a model with six interlayer exchange interactions, here we investigate by MC simulations the properties of the same system by making use of the simplest model Hamiltonian able to describe the onset of a helical magnetic order in Holmium, i.e. we consider only two inter-layer coupling constants, as previously done in Ref. 11.

The paper is organized as follows: In Sec. II the model Hamiltonian will be defined, and the MC techniques, and all the thermodynamic quantities relevant for this study, will be introduced. In Sec. III the results obtained for different thicknesses will be presented, both in the matter of the critical properties of the model and of the magnetic ordered structures observed. Finally, in Sec. IV we shall discuss such results, drawing also some conclusions.

## II. MODEL HAMILTONIAN AND MONTE CARLO OBSERVABLES

The model Hamiltonian we use in our simulations is the minimal one able to describe helimagnetic structures:

$$\mathcal{H} = - \left[ J_0 \sum_{\langle ij \rangle} \vec{S}_i \cdot \vec{S}_j + J_1 \sum_{\langle ik \rangle} \vec{S}_i \cdot \vec{S}_k + J_2 \sum_{\langle il \rangle} \vec{S}_i \cdot \vec{S}_l \right]. \quad (1)$$

$\vec{S}_i$  are classical planar unit vectors representing the direction of the total angular momentum of the magnetic ions, whose magnitude  $\sqrt{j(j+1)}$  ( $j = 8$  for Holmium ions) is already encompassed within the definition of the interaction constants  $J_{0,1,2}$ . As sketched in Fig. 1, the magnetic ions are located on the sites of a body-centered tetragonal (BCT) lattice; the first sum appearing in the Hamiltonian describes the in-plane ( $xy$ ) nearest neighbor (NN) interaction, which is taken ferromagnetic (FM), with exchange strength  $J_0 > 0$ ; the second sum represents the coupling, of exchange strength  $J_1$ , between spins belonging to nearest neighbor (NN) planes along the  $z$ -direction (which we will assume to coincide with the film growth direction); finally, the third sum takes into account the interaction, of exchange strength  $J_2$ , between spins lying on next-nearest neighbor (NNN) planes along  $z$ . In order to have frustration, giving rise to non-collinear order along  $z$  in the bulk, NN interaction  $J_1$  can be taken both ferro- or antiferromagnetic, but NNN coupling  $J_2$  has necessarily to be antiferromagnetic, and the condition  $|J_2| > |J_1|/4$  must be fulfilled. Such simplified Hamiltonian was already employed to simulate helical ordering in bulk systems by Diep<sup>1,17</sup> and Loison<sup>18</sup>. In the bulk limit, the state of minimal energy of a system described by Eq.(1) corresponds to a helical arrangement of spins. The ground state energy per spin is equal to  $e_g(Q_z) = [-4J_0 - 2J_1(4 \cos(Q_z c') + \delta \cos(2Q_z c'))]$  where  $c'$  is the distance between NN layers,  $\delta = \frac{J_2}{J_1}$ , and  $Q_z c' = \arccos(-\frac{1}{\delta})$  is the angle between spins lying on adjacent planes along the  $z$ -direction. The observed helical arrangement in bulk holmium corresponds to  $Q_z c' \simeq 30.5^\circ$ <sup>10</sup>: such value can be obtained from the formula above with the set of coupling constants  $J_0=67.2\text{K}$ ,  $J_1=20.9\text{K}$ , and  $J_2 = -24.2\text{K}$ , that we have employed in our simulations. The given values for the exchange constants are the same already used by Weschke *et al.* in Ref. 13 to interpret experimental data on Holmium films on the basis of a  $J_1 - J_2$  model, after a proper scaling by the numbers of NN and NNN on neighboring layers of a BCT lattice.

In the following we will denote with  $n$  the film thickness, i.e. the number of spin layers along the  $z$  direction, and with  $L \times L$  the number of spins in each layer (i.e.,  $L$  is the lattice size along both the  $x$  and  $y$  directions). In our simulations thickness values from 1 to 24 were considered, while the range of lateral size  $L$  was from 8 to 64. Periodic boundary conditions were applied along  $x$  and  $y$ , while free boundaries were obviously taken along the film growth direction  $z$ .

Thermal equilibrium was attained by the usual Metropolis algorithm<sup>19</sup>, supplemented by the over-relaxed technique<sup>20</sup> in order to speed-up the sampling of the spin configuration space: a typical “Monte Carlo step” was composed by four Metropolis and four-five over-relaxed moves per particle. Such judicious mix of moves is able both to get faster the thermal equilibrium and to minimize the correlation “time” between successive samples, i.e. the undesired effects due to lack of in-

dependence of different samples during the measurement stage. For each temperature we have usually performed three independent simulations, each one containing at least  $2 \times 10^5$  measurements, taken after discarding up to  $5 \times 10^4$  Monte Carlo steps in order to assure thermal equilibration.

In the proximity of the critical region the multiple histogram (MH) technique was also employed<sup>21</sup>, as it allows us to estimate the physical observables of interest over a whole temperature range in a substantially continuous way by interpolating results obtained from sets of simulations performed at some different temperatures.

For all the quantities of interest, the average value and the error estimate were obtained by the bootstrap re-sampling method<sup>22</sup> given that, as pointed out in Ref. 23, for a large enough number of measurements, this method turns out to be more accurate than the usual blocking technique. In our implementation, we pick out randomly a sizable number of measurements (typically, between 1 and  $1 \times 10^3$  for the single simulation, and between 1 and  $5 \times 10^4$  for the MH technique), and iterate the re-sampling at least one hundred times.

The thermodynamic observables we have investigated include the FM order parameter for each plane  $l$ :

$$m_l = \sqrt{(m_l^x)^2 + (m_l^y)^2} \quad , \quad (2)$$

which is related to the  $SO(2)$  symmetry breaking. At the same time, it turns out to be significant also the average order parameter of the film, defined as

$$M = \frac{1}{n} \sum_{l=1}^n m_l \quad . \quad (3)$$

Turning to the helical order, which is the relevant quantity for the  $\mathbb{Z}_2 \times SO(2)$  symmetry, we can explore it along two different directions. The first one is by the introduction of the chirality order parameter<sup>1,2</sup>

$$\kappa = \frac{1}{4(n-1)L^2 \sin Q_z} \sum_{\langle ij \rangle} [S_i^x S_j^y - S_i^y S_j^x] \quad , \quad (4)$$

where the sum refers to spins belonging to NN layers  $i$  and  $j$ , respectively, while  $Q_z$  is the bulk helical pitch vector along the  $z$  direction. The second possibility is that of looking at the integral of the structure factor:

$$M_{HM} = \frac{1}{K} \int_0^\pi dq_z S(\vec{q}) \quad (5)$$

where  $S(\vec{q})$ , with  $\vec{q} = (0, 0, q_z)$ , is the structure factor<sup>24</sup> (i.e. the Fourier transform of the spin correlation function) along the  $z$ -direction of the film, while the normalization factor  $K$  is the structure factor integral at  $T = 0$ . Although the use of the last observable can be seen as a suitable and elegant way to overcome the intrinsic difficulties met in defining a correct helical order parameter, free of any undue external bias (as the wave-vector  $Q_z$

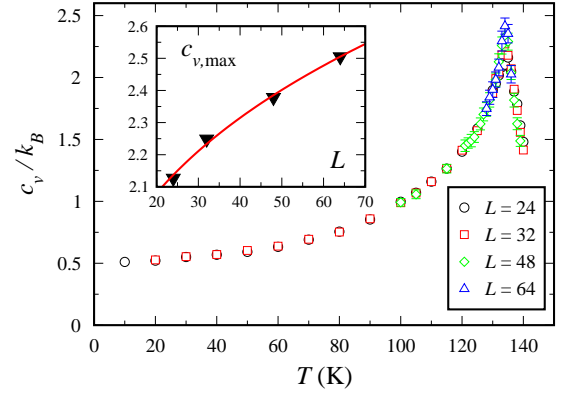


FIG. 2: (color online) Specific heat  $c_v$  per spin vs. temperature for thickness  $n = 16$  (for lateral dimension, see the legend inside the figure). Inset: Maximum of  $c_v$  vs.  $L$  obtained through MH technique. The continuum red line is a power law fit.

entering the definition of  $\kappa$  in Eq. (4)), we remind that such quantity has generally to be managed with particular care, as discussed in details in Refs.<sup>14,15</sup>, where it was shown that the presence of block structures prevents us to unambiguously relate the evolution of  $S(\vec{q})$  with the onset of helical order. However, for the specific case of the model under investigation such integrated quantity can still be considered a fairly significant order parameter, as no block structures emerge from the simulations (see below).

In order to get a clear picture of the critical region and to give an accurate estimate of the critical temperature, we look also at the following quantities

$$c_v = nL^2\beta^2 (\langle e^2 \rangle - \langle e \rangle^2) \quad , \quad (6)$$

$$\chi_o = nL^2\beta (\langle o^2 \rangle - \langle o \rangle^2) \quad , \quad (7)$$

$$\partial_{\beta} o = nL^2 (\langle oe \rangle - \langle o \rangle \langle e \rangle) \quad , \quad (8)$$

$$u_4(o) = 1 - \frac{\langle o^4 \rangle}{3\langle o^2 \rangle^2} \quad , \quad (9)$$

where  $\beta = 1/k_B T$ , and  $o$  is one of the relevant observables, i.e.  $m_l, M, \kappa, M_{HM}$ . In this paper, we shall mainly locate the critical temperature by looking at the intersection of the graphs of the Binder cumulant<sup>25</sup>, Eq. (9), as a function of  $T$  obtained at different  $L$ . For clarity reasons, we introduce also the following symbols: by  $T_N(n)$  we will denote the helical/fan phase transition temperature for thickness  $n$ ,  $T_C(n)$  will instead indicate the ordering temperature of the sample as deduced by looking at the behaviour of the average order parameter (3), while  $T_C^l(n)$  will be the  $l$ -th plane transition temperature related to the order parameter defined in Eq. (2).

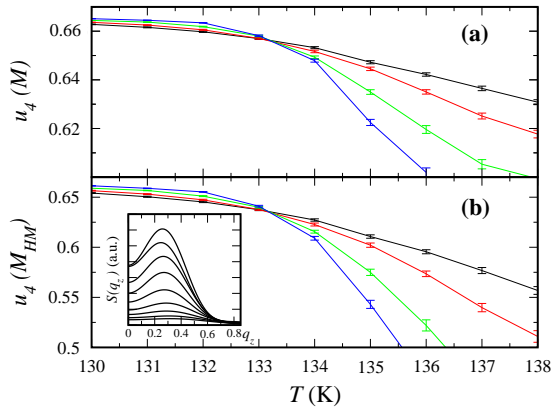


FIG. 3: (color online) Binder cumulants at thickness  $n = 16$ , colors as in Fig. 2. (a): Binder cumulant for the order parameter defined in Eq. (3). (b): Binder cumulant extracted from the integral of the structure factor (see Sec. II). Inset: structure factor for  $L = 64$  between  $T = 131$  K (upper curve) and  $T = 140$  K (lower), with 1 K temperature step.

### III. RESULTS

The results obtained by MC simulations of the model introduced in Sec. II will be presented starting from  $n = 16$ , i.e. the highest investigated film thickness which still displays a bulk-like behaviour. In Fig. 2 the specific heat for samples with  $n = 16$  and lateral dimension  $L = 24, 32, 48, 64$  is shown. The location of the specific heat maximum shows a quite definite evolution toward the bulk transition temperature,  $T_N^{Ho} \simeq 132$  K<sup>10</sup> (it is worthwhile to note that for this XY model the mean field theory predicts a critical temperature  $T_{N,MF}^{Ho} \simeq 198$  K).

The intensity of the maximum of  $c_v$  has been analyzed by the MH technique for the same lateral dimensions (see inset of Fig. 2): it clearly appears as it increases with  $L$  in a smooth way.

The Binder cumulant for the average order parameter defined in Eq. (3) was obtained close to the  $c_v$  peak and is reported in Fig. 3a; its analysis leads to an estimate of the critical temperature of the sample (given by the location of the common crossing point of the different curves reported in the figure) of  $T_C(16) = 133.2(5)$ . This value can be considered in a rather good agreement with the experimental ordering temperature of Holmium  $T_N^{Ho}$ , the relative difference being about 1%. Even such a mismatch between  $T_N^{Ho}$  and  $T_C(16)$  could be completely eliminated by slightly adjusting the in-plane coupling constant  $J_0$ , but, as discussed in Sec. II, we shall preserve the value reported in Refs. 13, and 12 in order to allow for a correct comparison with the results reported in those papers.

The development of the helical arrangement of magnetization along the film growth direction was investigated by looking at the integral of the structure factor  $S(\vec{q})$  along the  $z$ -direction, i.e. by taking  $\vec{q} = (0, 0, q_z)$ , and making again use of the cumulant analysis in order to locate the helical transition temperature at  $T_N(16) =$

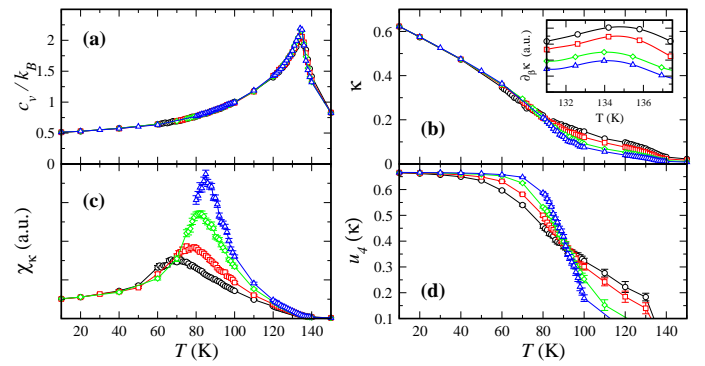


FIG. 4: (color online) Thermodynamic quantities obtained for thickness  $n = 8$  in the temperature range 0-150 K. Colors and symbols as in Fig. 2. (a): specific heat; (b): chirality order parameter. (c): susceptibility  $\chi_\kappa$ . (d): Binder cumulant for  $\kappa$ .

133.1(3) K (see Fig. 3b). The crossing points of the Binder's cumulants of the helical order parameter immediately appear to be located, within the error bars, at the same temperature of those for the average magnetization previously discussed. In addition, it is worthwhile to observe that the peak evolution of  $S(0, 0, q_z)$ , in particular close to  $T_N(16)$  (inset of Fig. 3b), displays the typical behaviour expected for an helical structure. We can thus conclude that for  $n = 16$ , as it is commonly observed in bulk samples, the establishment of the in-plane order coincides with onset of the perpendicular helical arrangement at  $T_N(16)$ . However, due to helix distortion in the surface regions, the maximum of  $S(0, 0, q_z)$  stabilizes at values of  $q_z$  sensibly smaller (e.g.  $Q_z(T_N(16)) \approx 16^\circ$ , and  $Q_z(T = 10K) \approx 28^\circ$ ) with respect to the bulk one ( $Q_z^{Ho} = 30.5^\circ$ ).

The MC simulations outcomes for  $n = 16$  we just presented appear quite different with respect to those obtained at the same thickness for the model with six coupling constants along the  $z$  direction<sup>14,15</sup>. Indeed, for the  $J_1$ - $J_2$  model here investigated, we observe that all layers order at the same temperature, and we do not find any hint of the block-phase, with inner disordered planes intercalated to antiparallel *quasi*-FM four-layer blocks, previously observed; sample MC runs we made using the same *hcp* lattice employed in Refs. 14,15 shows that the presence or absence of the block phase is not related to the lattice geometry, but it is a consequence of the interaction range only.

We now move to describe and discuss MC simulation data for thinner samples. A graphical synthesis of the results obtained for  $n = 8$  is reported in Fig. 4a-d. The specific heat  $c_v$ , shown in Figs. 4a, reveals very small finite-size effects, which, however, cannot be unambiguously detected for the largest lattice size ( $L = 64$ ), as they fall comfortably within the error range. Surprisingly, the specific heat maximum is located close to the bulk transition temperature as found for  $n = 16$ , and

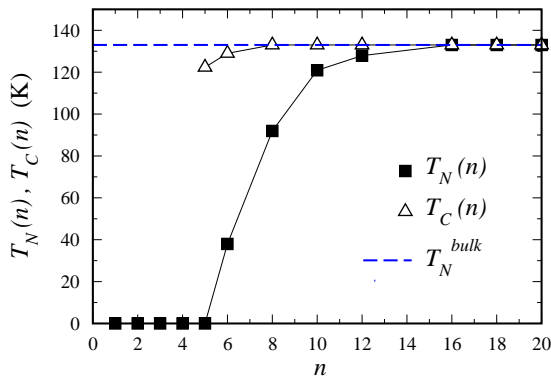


FIG. 5: Transition temperatures  $T_N(n)$  and  $T_C(n)$  vs. film thickness  $n$ .

the same is true for the crossing point of the Binder cumulant of the average magnetization  $M$  (not reported in figure), which is located at  $T_C(8) = 133.3(3)$  K. These data give a first rough indication that also for  $n = 8$  all the planes of the sample are still ordering almost at the same temperature; such property has been observed for all the investigated thicknesses  $n$  below 16, so that  $T_C(n)$  results quite  $n$ -independent (see also Fig. 5).

Although the layer subtraction does not seem to modify  $T_C(n)$ , the onset of helical arrangement is observed to shift at lower temperatures as  $n$  decreases. The chirality  $\kappa$  defined in Eq. (4) is reported in Fig 4b for  $n = 8$ . As the temperature decreases, around  $T \sim 80$  K we can identify a finite-size behaviour of  $\kappa$  which, at variance with the previous one, can be easily recognized as typical of an effective phase transition. Such conclusion is confirmed by the analysis of the chiral susceptibility  $\chi_\kappa$  (Fig. 4c), which for the largest  $L$  has a maximum at  $T = 85$  K. Assuming that the order parameter (4) is the relevant one to single out the onset of the fan arrangement, we can get a more accurate estimate of  $T_N(8)$  by looking at the Binder cumulant  $u_4(\kappa)$ , reported in Fig. 4d. By making use of the MH technique, we locate the crossing point at  $T_N(8) = 92(2)$  K. Finally, it is worthwhile to observe as the specific heat does not show any anomaly at  $T_N(8)$ , being the entropy substantially removed at  $T_C(8)$ .

The scenario just outlined for  $n = 8$  results to be correct in the thickness range  $6 \leq n \lesssim 15$ , where a clear separation between  $T_N(n)$  and  $T_C(n)$  can be easily figured out. In such temperature window, the strong surface effects produce a *quasi*-FM set-up of the magnetic film structure along the  $z$ -direction. While leaving to the next Section a more detailed discussion of this regime, we report in Fig. 5 a plot of  $T_N(n)$  and  $T_C(n)$  vs.  $n$  for all the simulated thicknesses. The separation between the two critical temperatures is maximum for  $n = 6$ , where  $T_N(6) = 38(4)$ , that is  $T_N(6) \sim \frac{1}{3}T_C(6)$ . For films with less than six layers no fan order is observed, i.e. for  $n = 5$  and below the chirality does not display any typical feature of fan ordering at any temperature below  $T_C(n)$ . As a representative quantity we finally look at the rotation

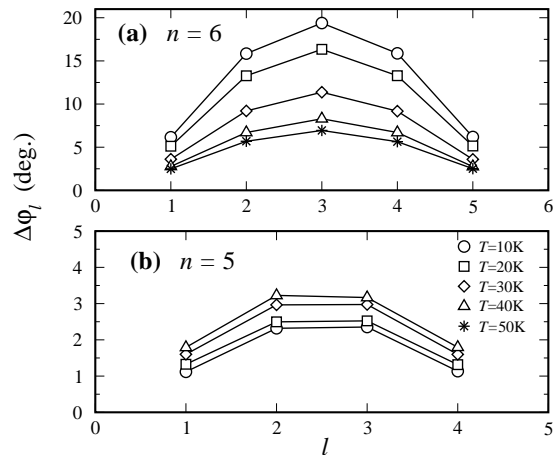


FIG. 6: Rotation angle  $\Delta\varphi_l$  between magnetic moments on NN layers  $(l+1, l)$  at some low temperatures, for thickness  $n = 5$  and  $n = 6$ , and lateral dimension  $L = 64$ .

angle of the magnetization between nearest planes:

$$\Delta\varphi_l = \varphi_{l+1} - \varphi_l = \arccos [M_l^x M_{l+1}^x + M_l^y M_{l+1}^y] \quad (10)$$

where  $(M_l^x, M_l^y)$  is the magnetic vector profile for each plane  $l$ .  $\Delta\varphi_l$  is displayed in Fig. 6a and Fig. 6b, for  $n = 6$  and  $n = 5$ , respectively. In Fig. 6a, a quite clear fan stabilization is observed when the temperature decreases, while in Fig. 6b, i.e. for  $n = 5$ ,  $\Delta\varphi_l$  keeps an almost temperature independent very small value; what's more,  $\Delta\varphi_l$  seems to loose any temperature dependence as  $T = 0$  is approached. We attribute the absence of fan arrangement for  $n \leq 5$  as simply due to the lack of “bulk planes” inside the film, so that we are left with only a 2d trend at  $T_C(n)$ , i.e. at the temperature where the order parameters defined in Eqs. (2) and (3) show a critical behaviour.

#### IV. DISCUSSION AND CONCLUSION

A possible framework to analyze the results presented in the previous Section is suggested by Fig. 5, where we can easily distinguish three significant regions: *i*) high thickness,  $n \geq 16$ , where the films substantially display a bulk behaviour, with the single planes ordering temperature coinciding with the helical phase transition one; *ii*) intermediate thickness,  $6 \leq n \lesssim 15$ , where the temperature corresponding to the onset of in-plane order,  $T_C(n)$ , is still  $\simeq T_N^{Ho}$ , but where the helical/fan arrangement stabilizes only below a finite temperature  $T_N(n) < T_C(n)$ ; *iii*) low thickness,  $1 \leq n \leq 5$ , where  $T_C(n) \lesssim T_N^{Ho}$  but no fan phase is present at any temperature.

The observed behaviour in region *iii*) can be reasonably attributed to the decreasing relevance of the contribution to the total energy of the system coming from the competitive interactions among NNN planes as the film thickness decreases; moreover, the thinness of the

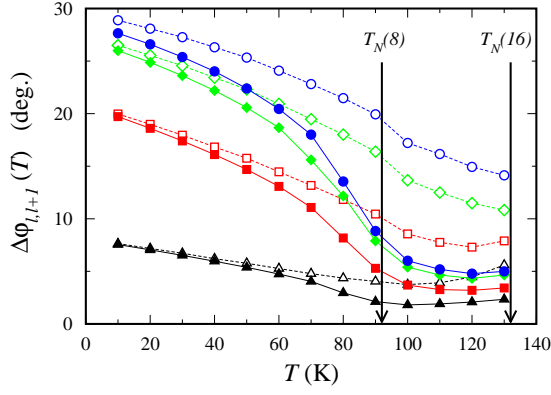


FIG. 7: (color online)  $\Delta\varphi_l(T)$  vs. temperature for the surface planes,  $l = 1$  (triangles),  $l = 2$  (squares),  $l = 3$  (diamonds),  $l = 4$  (circles). Straight lines and full symbols:  $n = 8$ . Dashed lines and open symbols:  $n = 16$ .

film leads to an effective 2d-like trend. Region *ii*) looks however more intriguing, and requires a more accurate discussion, which can benefit from a careful comparison of the behaviour of a given quantity in regions *i*) and *ii*).

For this purpose, we look at the temperature dependence of the rotation angle of the magnetization between NN planes. In Fig. 7,  $\Delta\varphi_l(T)$  for  $n = 8$  and  $n = 16$  (continuous and dashed lines, respectively), is plotted for the outermost planes,  $l = 1 \dots 4$ . For both thicknesses, a monotonic trend is observed for all  $l$ , but at variance with what happens for the highest thickness, for  $n = 8$  we see, starting from a temperature  $T \lesssim T_N(8)$ , an abrupt drop of  $\Delta\varphi_3$  and  $\Delta\varphi_4$ , which rapidly reach an almost constant value, only slightly larger than  $\Delta\varphi_1$ . In the temperature range  $T_N(8) \lesssim T < T_C(8)$  we thus substantially observe the same small magnetic phase shifts between all NN layers, testifying an energetically stable *quasi*-FM configuration giving no contribution to the helical order parameters. The latter point can be made clearer by looking at the the peak position  $Q_{z,max}$  of the structure factor  $S(0,0,q_z)$ . In Fig. 8 the average of  $Q_{z,max}$  vs  $T$  is reported, again for  $n = 8$  and for different lateral dimensions  $L^{26}$ . As expected from the previous argument, we see that  $Q_{z,max} = 0$  for  $T_N(8) < T < T_C(8)$ , while it begins to shift to higher values as soon as the temperature decreases below  $T_N(8)$ , making apparent a progressive fan stabilization with  $Q_{z,max} \neq 0$  and reaching a value of about  $21^\circ$  for  $T = 10$  K.

In a previous study, where the magnetic properties of Ho thin films were investigated by MC simulations of a Heisenberg model with easy-plane single-ion anisotropy and six out-of-plane coupling constants (as obtained by experimental neutron scattering measurements<sup>16</sup>) on a HCP lattice<sup>14,15</sup>, it was found that for thicknesses comparable with the helical pitch the phase diagram landscape is quite different from what we find here. Indeed, for  $n = 9 - 16$ , three different magnetic phases could be sin-

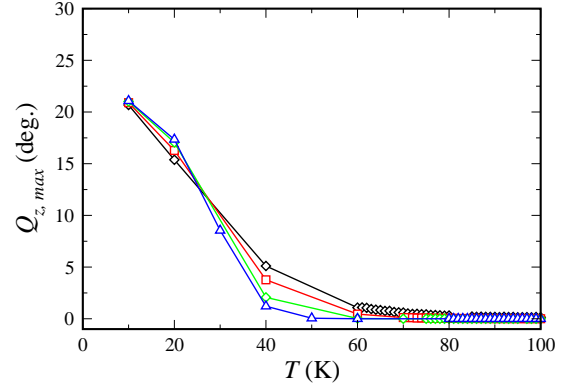


FIG. 8: (color online)  $Q_z$ , position of the maximum of  $S(\vec{q})$ , vs. temperature for thickness  $n = 8$ . Inset: magnetic vector  $(m_i^x, m_i^y)$  profile for some temperatures for  $L = 64$ . Colors and symbols as in Fig. 2.

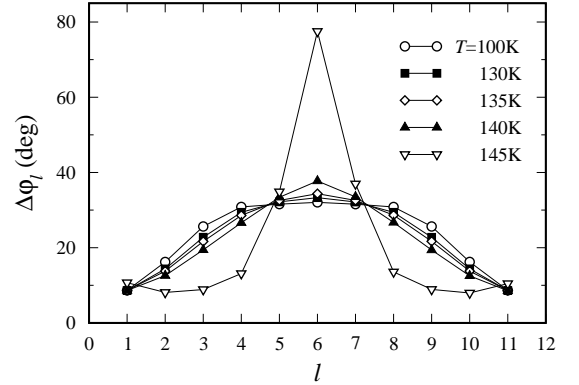


FIG. 9:  $\Delta\varphi_l$  for a BCT lattice and  $n = 12$ , when the six coupling constants set employed in Ref. 14,15 (see text) is used. The temperature range has been chosen around  $T_C(n)$  (error bars lie within point size).

gled out, with the high-temperature, paramagnetic phase separated from the low-temperature, long-range ordered one, by an intermediate-temperature block phase where outer ordered 4-layers blocks coexist with some inner disordered ones. Moreover, it was observed that the phase transition of such inner layers turns out to have the signatures of a Kosterlitz-Thouless one.

The absence of the block phase in the  $J_1 - J_2$  model here investigated has to be attributed to the different range of interactions, rather than to the different lattice structure. We came to this conclusion by doing some simulations using the same set of interaction constants employed in Refs. 14,15, but using a BCT lattice: the results we obtained for  $\Delta\varphi_l$  with  $n = 12$  are reported in Fig. 9. The latter is absolutely similar to Fig. 7 of Ref. 15 and clearly displays the footmarks of the block phase (see down-triangle), with two external blocks of ordered layers ( $l = 1 \dots 5$  and  $8 \dots 12$ ), where  $\Delta\varphi_l$  is roughly  $10^\circ$ , separated by a block of disordered layers, and with almost

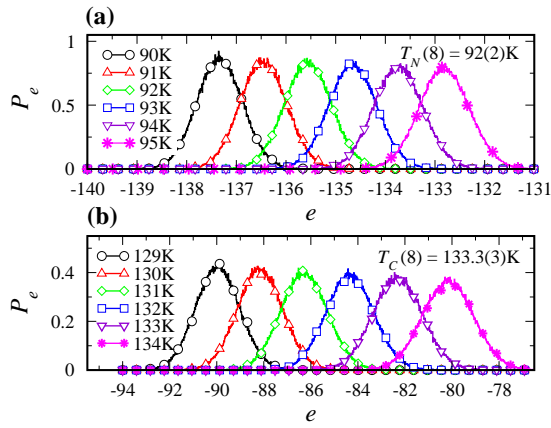


FIG. 10: (colors online) Equilibrium probability distribution of the energy for the thickness  $n = 8$  for some temperatures around  $T_N(8)$ , (a), and  $T_C(8)$ , (b), respectively.

opposite magnetization. We can thus confidently assert that, regardless of the underlying lattice structure, by decreasing the number of the out-of-plane interactions, for thicknesses close to the helical bulk pitch, the block

phase is replaced by a *quasi*-FM configuration in the intermediate temperature range  $T_N(n) < T < T_C(n)$ .

As a final issue we address the problem of the order of the transitions observed at  $T_N(n)$  and  $T_C(n)$ , respectively. In particular, we focus our attention to the thickness ranges where the chiral order parameter is relevant, i.e. regions *i*) and *ii*) as defined at the beginning of this Section. In Fig. 10 the equilibrium probability distribution of the energy for temperatures around  $T_N(8)$  (Fig. 10a) and  $T_C(8)$  (Fig. 10b) is plotted: for both temperatures, no double peak structure is observed, so that we have no direct indication for a first order transition even if, according to precedent studies of Loison and Diep<sup>17,18</sup>, the presence of a first-order transition at  $T_N(n)$ , cannot be completely excluded, as it could reveal itself only when the lateral dimension  $L$  are much larger than the largest correlation length. The same conclusion about the order of transition is reached for any other investigated film thickness, as the energy probability distribution shape does not qualitatively change. This findings agree with the results we got in previous MC simulations discussed in Ref. 15, so that we may conclude that the order of the observed transitions is not affected by the range of interactions.

- <sup>1</sup> *Frustrated spin Systems*, edited by H. T. Diep (World Scientific, 2004).
- <sup>2</sup> H. Kawamura, J. Phys.: Cond. Matt. **10**, 4707 (1998).
- <sup>3</sup> T. Kimura *et al.*, Nature (London) **426**, 55 (2003).
- <sup>4</sup> F. Cinti *et al.*, Phys. Rev. Lett. **100**, 057203 (2008).
- <sup>5</sup> J.H. Park, S. Onoda, N. Nagaosa, and J. H. Han, Phys. Rev. Lett. **101**, 167202 (2008), and references therein.
- <sup>6</sup> S. W. Cheong and M. Mostovoy, Nature Materials (London) **6**, 13 (2007).
- <sup>7</sup> Minhyea Lee, W. Kang, Y. Onose, Y. Tokura, and N. P. Ong, Phys. Rev. Lett. **102**, 186601 (2009).
- <sup>8</sup> P. Pedrazzini *et al.*, Phys. Rev. Lett. **98**, 047204 (2007).
- <sup>9</sup> H. Kawamura and M. S. Li, Phys. Rev. Lett. **87**, 187204 (2001).
- <sup>10</sup> P. J. Jensen, and A. R. Mackintosh, *Rare Earth Magnetism (Structure and Excitations)*, Clarendon Press, Oxford (1991).
- <sup>11</sup> S. Konings, C. Schuessler-Langeheine, H. Ott, E. Weschke, E. Schierle, J. B. Goedkoop, arXiv 0707.2765v2
- <sup>12</sup> P.J. Jensen, and K.H. Bennemann, Surface Science Reports **61**, 129 (2006).
- <sup>13</sup> E. Weschke, *et al.*, Phys. Rev. Lett. **93**, 157204 (2004).
- <sup>14</sup> F. Cinti, A. Cuccoli, and A. Rettori, Phys. Rev. B **78**, 020402(R) (2008).
- <sup>15</sup> F. Cinti, A. Cuccoli, and A. Rettori, Phys. Rev. B **79**, 134420 (2009).
- <sup>16</sup> J. Bohr D. Gibbs, J. D. Axe, D. E. Moncton, K. L. D'Amico, C. F. Majkrzak, J. Kwo, M. Hong, C. L. Chien, and J. Jensen, Physica B **159**, 93 (1989).
- <sup>17</sup> H. T. Diep, Phys. Rev. B **39**, 397 (1989).
- <sup>18</sup> D. Loison, Physica A **275**, 207 (2000).
- <sup>19</sup> N. Metropolis, *et al.*, J. Chem. Phys. **21**, 1087 (1953).
- <sup>20</sup> F. R. Brown and T. J. Woch, Phys. Rev. Lett. **58**, 2394 (1987).
- <sup>21</sup> D. P. Landau, and K. Binder, *A Guide to Monte Carlo Simulation in Statistical Physics*, Cambridge University Press, Cambridge (2000).
- <sup>22</sup> M. E.J. Newman, and G. T. Barkema, *Monte Carlo Methods in Statistical Physics*, Clarendon Press, Oxford (1999).
- <sup>23</sup> B. Efron, The Annals of Statistics **7**, 1 (1979).
- <sup>24</sup> P. M. Chaikin, T. C. Lubensky *Principles of condensed matter physics*, Cambridge University Press, New York (1995).
- <sup>25</sup> K. Binder, Z. Phys. B **43**, 119 (1981). K. Binder, Phys. Rev. Lett. **47**, 693 (1981).
- <sup>26</sup> Such observable has been obtained from instantaneous evaluation of the structure factor during the stochastic process, and subsequently statistically analyzed as all the other macroscopic quantities.